Changes in Size-Resolved Particle Composition Linked with Meteorology Measurements and Air Mass Back Trajectories to Increase Understanding of Sources and Secondary Contributions to Particulate Matter

9. Characterization of trace metals in single urban particles during the SOAR 2005 campaign

i. Introduction

Now that epidemiologic studies have substantiated an association between increased exposure to particulate matter (PM) and risk for cardiopulmonary disease and mortality (280), the next step for research studies is to improve the overall understanding of the mechanisms and specific physical and chemical PM characteristics are causing these human health effects. Recent studies have linked exposure to trace metal-rich ambient PM with acute airway inflammation, which likely induces chronic diseases (281) and potentially causes mortality and morbidity (282). Greater knowledge of the sources, transformations, and fates of these metal-containing particles also will clarify their impact on the environment. Trace metals are distributed in the urban environment by natural processes (including wind erosion, volcanism, and biomass burning) as well as anthropogenic activities (such as fossil fuel combustion, municipal waste disposal, industrial metallurgical processes, and wear of vehicular and construction materials) (283). In the atmosphere, even a small presence of transition metal ions in particles can influence cloud chemistry (284). Dry and wet deposition of PM also constitute a major load of trace metal contamination to soils, agroecosystems, and aquatic systems (283,285). Deposition processes can contribute as much as 57-100% of the trace metals in stormwater in semi-arid regions such as southern California (286). These health and environmental ramifications warrant detailed analysis of ambient metal-containing particles.

Most data on trace metals in PM have been obtained from bulk filter analysis; the results are informative, although the approach has some caveats. Depending upon the sensitivity of the analytical technique, the low metal mass concentrations require collection times of varying lengths, often as long as 24 hours, for sufficient detection. Before measurement, the PM-loaded substrates must undergo precise multi-step extraction procedures to reduce the loss of sample (287,288). Online aerosol instrumentation offer an alternative approach which avoids many of these sampling artifacts and limitations and yields high temporally resolved data, which once correlated with wind speed and direction can locate potential sources (289). Moreover, techniques like single particle mass spectrometry (SPMS) provide detailed chemical analysis on the individual particle level with better statistical representation than other single particle methods, such as scanning electron microscopy (SEM) (290,291). SPMS data help decipher the chemical complexity of aerosols, granting insight into how trace metals in PM are damaging human health and the environment. Though SPMS techniques are not as quantitative as bulk filter methods, they do provide “fingerprints” and the chemical

species with which the metals are associated – key information for determining the sources of metal-containing particles.

This study employs an SPMS technique, known as aerosol time-of-flight mass spectrometry (ATOFMS), to determine the chemical speciation of size-segregated trace metal-containing urban ambient particles in southern California. ATOFMS simultaneously acquires positive and negative ion spectra, as well as size information, for single particles in real-time. Along with chemical speciation, the number concentrations, size, temporal trends, and wind directionality of trace metal-containing particles will be used to identify the most probable sources as well as gain insights into the short term variability of metal particles in urban air.

ii. Experimental

a. Sampling Location

Located approximately 80 km east of downtown Los Angeles, the city of Riverside, California commonly experiences air masses that have crossed the Los Angeles basin. Sampling occurred via a mobile laboratory on the campus of the University of California, Riverside (33°58′18″N, 117°19′22″W) in conjunction with the Study of Organic Aerosols at Riverside (SOAR) 2005 campaign. This work focuses on continuous data collected in the summer (July 30 - August 15) and fall (October 31 - November 21) seasons.

b. Instrumentation

Single particle size and chemical composition were measured by ATOFMS. Ultrafine ATOFMS (UF-ATOFMS) detected particles with aerodynamic diameters between 100 nm and 350 nm, while standard inlet ATOFMS measured particles with aerodynamic diameters between 300 nm and 2.5 µm. The trace metal-containing ultrafine particles (50-100 nm) detected by UF-ATOFMS were statistically too low to be included here. Details of the transportable instrumentation have been described previously (1,2). In this work, $PM_{2.5}$ refers to all particular matter in the aerodynamic size range of 100 to 2500 nm. To account for the ATOFMS size-dependent transmission efficiency, the number concentrations of ATOFMS chemical composition data could be scaled to concurrently-measured particle size distribution data, such as a scanning mobility particle sizer (SMPS) (36). As described in previous chapters, it has been shown that there can be sufficient size differences between the ATOFMS aerodynamic diameter and the SMPS mobility diameter for certain chemical particle types (48,292). Due to the limited knowledge of shape factor and density values for the specific trace metal-containing particle types in Riverside during this campaign, the ATOFMS data were not scaled and are presented in raw counts in this study. Suitable scaling conversions between aerodynamic and mobility diameters are still under development.

c. Data analysis

This study uses a similar data analysis approach to that of Tolocka and coworkers (291), which involves pre-selection of potential spectra before running a clustering algorithm. Because trace metal-containing particles represent only a small fraction of the millions of particle spectra collected during the SOAR campaigns, it was necessary to

isolate probable metal spectra based upon a relatively low threshold level for ion areas (peak area of 100) at the mass-to-charge ratio(s) (*m/z*) of the common isotope(s) (≥20% natural abundance) of the specified metal. For example, three of the four main lead isotopes have a natural abundance greater than 20% (^{206}Pb, ^{207}Pb, and ^{208}Pb), so only these three *m/z* values were used to extract the possible lead-containing particles. Once the potential spectra were pulled out, the adaptive resonance theory neural network algorithm, ART-2a, sorted and classified particles with similar spectral characteristics (35). The ART-2a learning rate, number of iterations, and vigilance factor (VF) were set to 0.05, 20, and 0.70, respectively, for this publication. This work focuses on the main metal types, and therefore it was not necessary to use a higher VF value to produce highly specific clusters, which are more commonly used in source characterization datasets for source apportionment studies. The VF value of 0.70 was sufficient to obtain distinct major classes. The resulting ART-2a clusters then were examined manually for the presence of trace metals, confirmed by the appropriate isotopic patterns and/or metal oxides. The trace metals examined in this study were V, Fe, Ni, Cu, Zn, Sr, Mo, Sn, Sb, Ba, W, and Pb.

iii. Results and Discussion

Though trace metal-containing particles generally represent small percentages of the overall PM, correlations between trace metals and other pollutants have made trace metal concentrations a potential air quality index (293,294). Day-of-week patterns in trace metal concentrations can provide insight into the ambient sources, particularly those based on dependent on human activities (295). For instance, high concentrations on working days (weekdays) and low concentrations on non-working days (weekends) indicate an anthropogenic source, particularly standard business hour facilities rather than continuously operating industries. Motor vehicle traffic is lightest on Sundays, and therefore, particle types with the lowest concentrations on Sundays compared to the rest of the week most likely originate from vehicle emissions. Nevertheless, it is important to consider that not only do vehicle emissions decrease with reduced traffic but so does re-suspended road dust (296). Alternatively, natural sources would be expected to have no day-of-week trends. However, when these considerations are applied to the bulk (24-hour) data, it can be difficult to identify strong day-of-week patterns for trace metals. This day-of-week bulk-analysis approach may not perform well for locations like Riverside, where multiple sources of trace metals can convolute the daily patterns. Such environments need more detailed analysis on smaller time scales.

One of the advantages of ATOFMS is high time resolution, so the dataset is not limited to 24-hour periods, as normally shown for metals. ATOFMS also yields highly resolved sizing data. Details on the size distribution of trace metal-containing ambient aerosols are informative from a health perspective as well as for understanding the atmospheric fate of these particles; the particle size determines the extent of its penetration into the airways or lungs and thereby the extent of its toxicity, and it also dictates the range of transport and deposition rate (297). In order to gain further insight into the temporal variability of metal-containing aerosols as well as their size, the following figures present high temporal (half-hour) resolution and size resolved number concentrations.

Because different particle classes can all contain the same trace metal, the metal-specific figures provide the detailed features for three main particle types, based on the ART-2a clusters, for each of the most abundant trace metals: vanadium, iron, zinc, barium, and lead. Nickel was excluded due to its correlation with vanadium, as explained below. Plots (a)-(c) of each figure show representative mass spectra for the main particle types. For each mass spectrum, the main ion m/z peaks are labeled, and the corresponding color is maintained throughout the remaining plots. The half-hourly ATOFMS counts for the types are displayed in plots (d) and (e) for the summer and fall seasons, respectively. These temporal plots utilize the same scale within each figure for easy seasonal comparison. The gray line tracks all particles containing the specified element to help illustrate how well the three types represent all particles with that metal. Breaks in the continuous traces indicate intervals in which the instruments were offline due to daily quality control checks or maintenance. The fractions each particle type represents relative to all chemically analyzed particles per size range are supplied in plots (f) and (g) for summer and fall, respectively. Again, the gray trace represents all particles containing that metal, and the scale ranges are the same within each figure. Finally, plots (h)-(j) show the wind directionality for each particle type, which can be used to help in identifying sources. The distance each symbol is from the origin signifies the magnitude of the specific metal-containing particle counts per half-hour bin, and the angle represents the direction from which the wind was coming during that half-hour. The open circle symbols indicate summer data, whereas the open triangles indicate fall data.

Vanadium and vanadium compounds are hazardous; in fact, the oxidized form of vanadium, vanadium pentoxide, is even more toxic than the elemental form (298). A study on urban particles around Seville, Spain determined that vanadium, compared to the other metals, had the highest percentage (50.4%) in the soluble and exchangeable fraction, meaning that vanadium is the most available metal to the human body via respiration (299). The properties of vanadium allow it to be employed in a variety of products: its strength and hardness are ideal for alloy formation, such as nickel/vanadium, ferrovanadium, and chrome/vanadium; industries like printing, textiles, and ceramics use it as a drying or reducing agent in paints, inks, dyes, and pigments; and finally, vanadium compounds also manifest in crude oils in the form of organic complexes (298). Thereby, human activities that rely on heavy oil combustion such as industrial boilers, ships, and power plants emit vanadium via residual fly ash (300-303). The dominant m/z peaks in the representative mass spectrum of Type V1 are vanadium [$^{+51}$V] and vanadium oxide [$^{+67}$VO] (**Figure 64**). Other positive ion peaks indicate the presence of iron [$^{+56}$Fe], nickel [$^{+58/60}$Ni], and carbonaceous species, mainly organic carbon (OC). The main negative ion species are nitrates ([$^{-46}NO_2$], [$^{-62}NO_3$], [$^{-}$

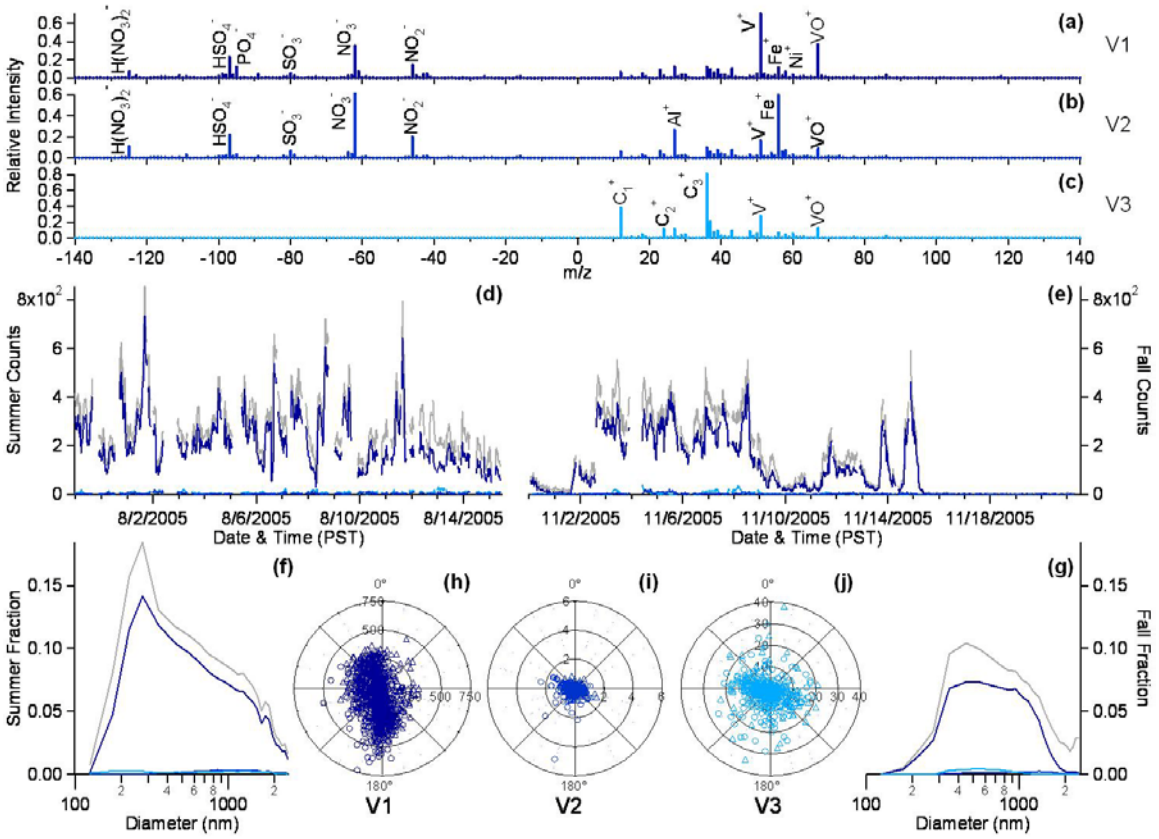

Figure 64: Trends of the three main vanadium particle types: representative mass spectra (a-c); half-hourly temporal variations in summer (d) and fall (e); size-resolved total particle fractions in summer (f) and fall (g); and half-hourly wind direction profiles based on particle counts (h-j).

$^{125}H(NO_3)_2$]) and sulfates ([$^{-80}SO_3$], [$^{-97}HSO_4$]). Type V1 is clearly the dominant vanadium particle class temporally for both seasons and across all sizes. Type V2 is similar to type V1, except that the inorganic species of iron and aluminum [^{+27}Al] are the dominant positive peaks for V2. However, type V2 tended to be observed in larger sized particles and was rarely observed by UF-ATOFMS which measures particles up to 350 nm. Type V2 could be agglomerates of type V1 with dust. Type V3 is an elemental carbon (EC) vanadium-containing particle class, as indicated by the intense carbon peaks of [$^{12}C^+$], [$^{24}C_2^+$], and [$^{36}C_3^+$] without strong OC ion peaks that are present in type V1. No negative ions were detected for this particle type which indicates these particles were heavily aged and had taken up water (304).

The two time series plots for vanadium demonstrate clear seasonal differences. In the overview of the general particle classes observed by ATOFMS during the SOAR campaigns, Qin and coworkers characterized ambient particle trends as diurnal for the summer season and episodic for the fall season (31). The vanadium particle classes appear to also follow the overall pattern of the ambient concentrations in both seasons, especially with the dramatic decline in number concentration during the Santa Ana periods (10/31-11/1 and 11/15-11/21). Occurring in the fall and early winter months, Santa Ana wind episodes bring warm and dry easterly winds to Southern California, which normally experiences westerly winds from over the Pacific Ocean. In the summer, the vanadium-containing $PM_{2.5}$ number concentrations tended to peak during the

afternoon and early evening hours. **Figure 65** and **Figure 66** include detailed plots on the local winds throughout both seasons. Westerly winds produced the highest wind speeds and were the dominant wind direction during daylight hours in the

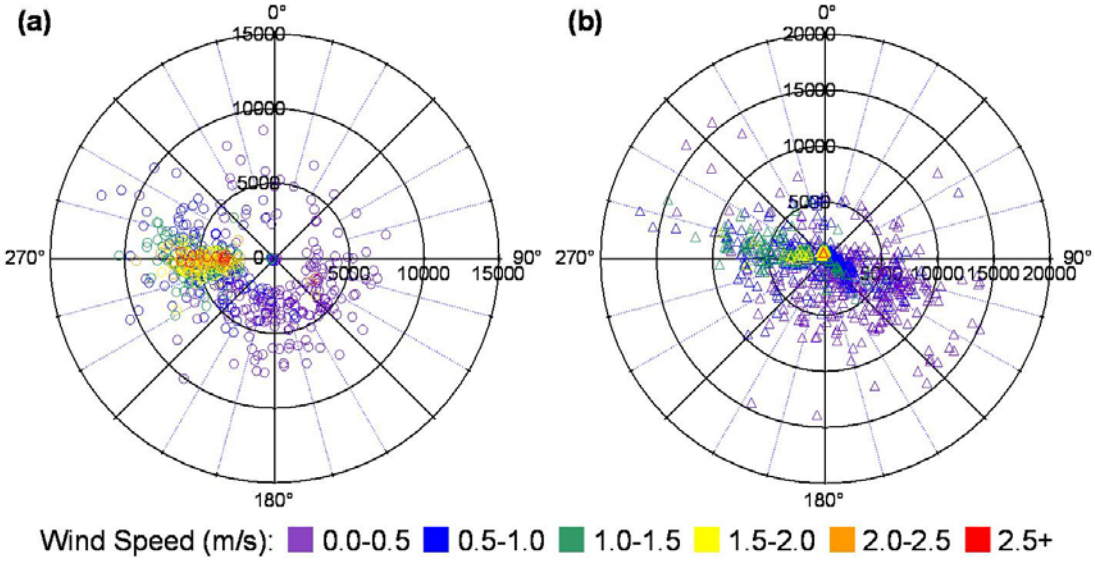

Figure 65: Half-hourly wind direction and wind speed (color scale) distribution for all $PM_{2.5}$ particle types in summer (a) and fall (b).

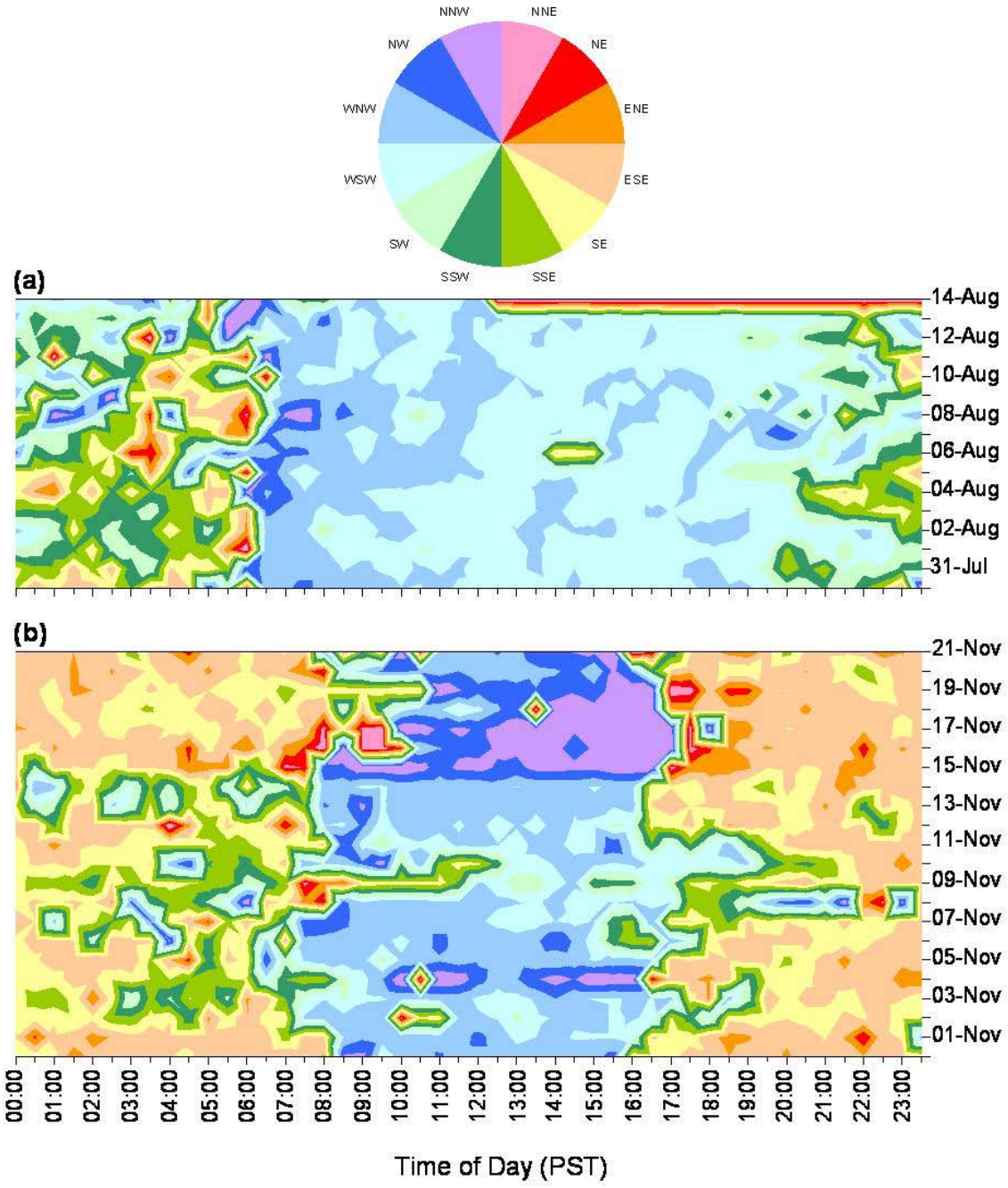

Figure 66: Half-hourly wind direction based on time of day for summer (a) and fall (b). Note that for the summer season, the meteorological data ended at 12:00 on August 14th.

summer. As shown in **Figure 64 h-j**, the wind direction plots specific to the particle types indicate foremost that vanadium-containing PM appear from all directions, since all the points are distributed around the center and there is no strong direction dependency based on the local winds. However, the plots do show more of a southwesterly/westerly direction dependency for the summer data (circles), which agrees with the vanadium-containing particles dominating during the afternoons when the westerly winds were the

strongest. The emissions from the millions of vehicles that drive daily in the south coast region as well as from the ships at the major shipping ports (Port of Los Angeles and Port of Long Beach) could travel east to the sampling site in Riverside (see the map in **Figure 67**). In fact, back trajectories from HYSPLIT (HYbrid Single-Particle Lagrangian Integrated Trajectory) model analysis (305) confirm that the air masses resulting in summertime V peaks passed over the major port and freeway areas of LA county before reaching Riverside. Currently, the source signatures for ship emissions are being investigated with a particular focus on the V particles (306).

Iron-containing urban particles have important influences on the surrounding environment; determining the solubility of iron-containing PM is a key piece of information for understanding the extent of which iron particles play a role in ocean productivity, which in turn impacts global climate (307). As expected, types Fe1 and Fe2 resemble types V1 and V2, because these particle types all contain vanadium and iron species (**Figure 68**). Additionally, the temporal trends, size profiles, and wind directionality also are similar to the corresponding V types. However, the mass spectrum for type Fe3 looks different; it contains more inorganic species, such

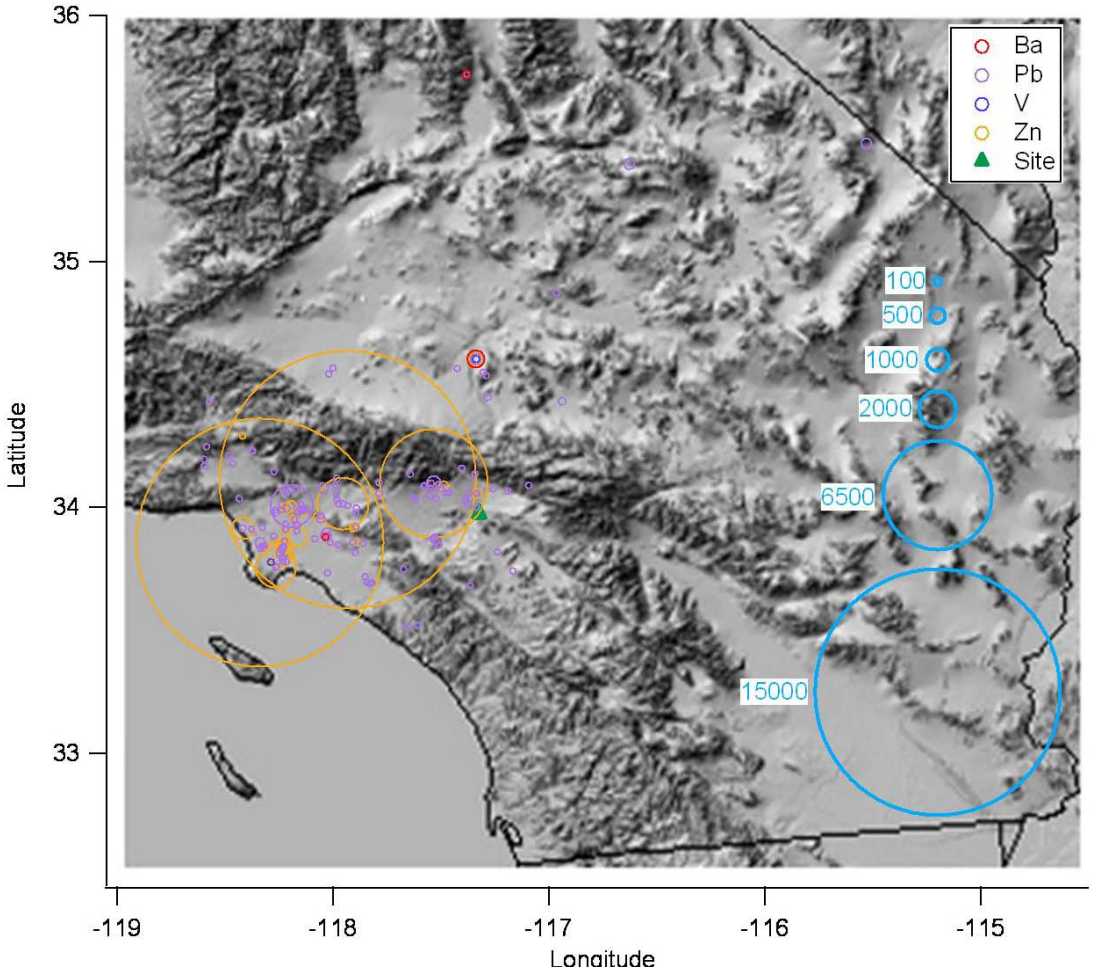

Figure 67: Reported annual atmospheric emissions of the specified metal and metal compounds in Riverside, Los Angeles, Orange, and San Bernardino counties in 2005 based on the data from the Environmental Protection Agency (EPA) Toxics Release Inventory (TRI).

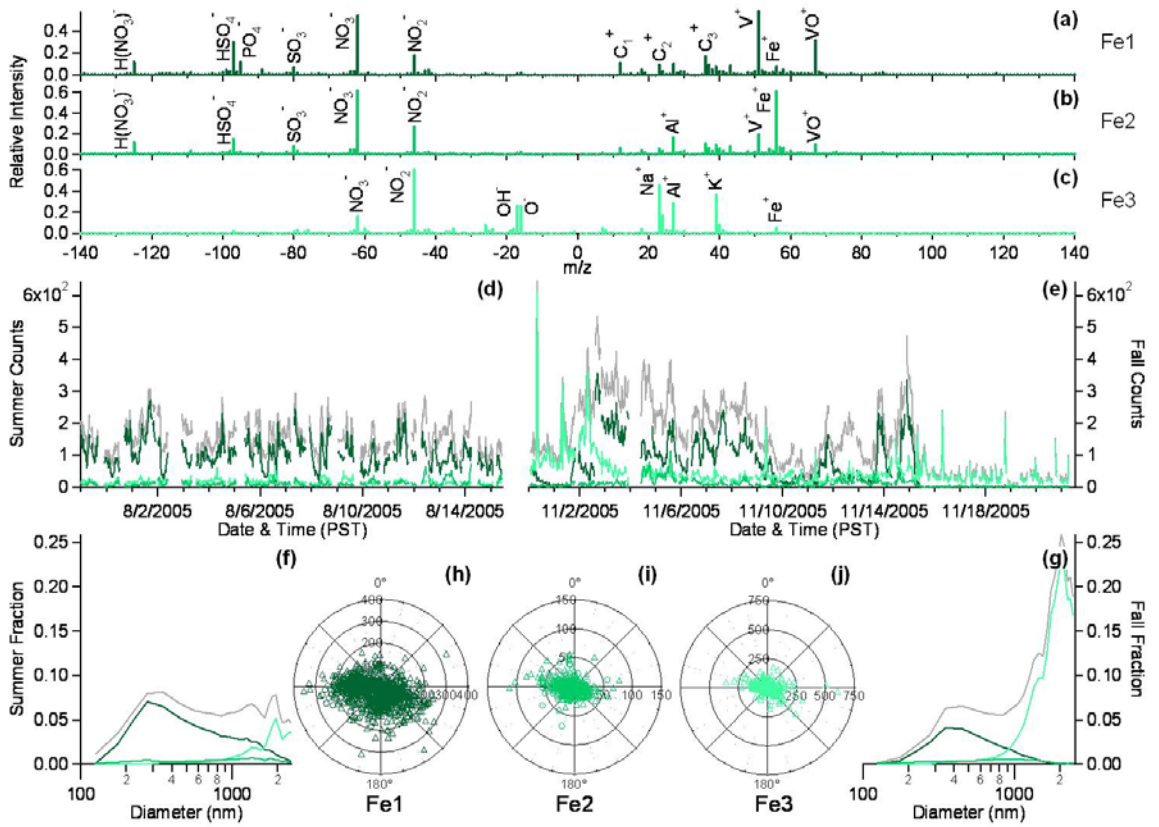

Figure 68: Trends of the three main iron particle types: representative mass spectra (a-c); half-hourly temporal variations in summer (d) and fall (e); size-resolved total particle fractions in summer (f) and fall (g); and half-hourly wind direction profiles based on particle counts (h-j).

as sodium [$^{+23}$Na], aluminum, and potassium [$^{+39}$K]. In addition to nitrates, the negative ions have oxygen [$^{-16}$O] and hydroxide [$^{-17}$OH] peaks. Type Fe3 is a dust particle class, and its size distribution is quite distinct when compared to the other metal types. The other profiles decrease sharply in the supermicron range, whereas the profile for type Fe3 remains increases with size; this size difference likely indicates the difference between metals of crustal origin, found in larger sized particles, and anthropogenic metals, found in smaller particles (308). Riverside particles that originate from urban Los Angeles anthropogenic sources are expected to be in the accumulation size mode due to the agglomeration of ultrafine and deposition of coarse particles via long-range transport (169). Because dust is generally resuspended PM, one might expect type Fe3 to be correlated with wind speed and direction; actually, most of the higher number concentrations of type Fe3 occurred when the local winds came from the east, particularly during the Santa Ana wind episodes in the fall season. According to the HYSPLIT results, the air masses with high Fe3 concentrations crossed desert areas east of the sampling site (Mojave Desert to the northeast and Sonoran Desert to the southeast). Zinc represents another major metal detected in particles during the fall and summer seasons. Hunt and coworkers examined archival lung tissues from humans known to have passed away from exposure during the 1952 London Smog in order to characterize the PM of this high mortality event captured within the lung compartments; they found evidence that Pb and Zn particle types in particular could be related to mortality (282).

Zinc is one of those biologically essential metals that has the potential for toxicity at high concentrations (283). Zinc-containing PM has several potential anthropogenic sources, such as tire wear, additives in lubricant oils, emissions from industries with galvanizing activities, and municipal and medical waste combustion emissions from incinerators (309,310). The type Zn1 mass spectrum shows the presence of sodium, potassium, zinc [$^{+64/66/68}$Zn], zinc chloride [$^{+99/101/103/105}$ZnCl], lead [$^{+206/207/208}$Pb], chloride [$^{-35/37}$Cl], nitrates, and phosphate [$^{-79}PO_3$] (**Figure 69**). Choel et al. studied the lead and zinc particle types downwind of a lead smelter and concluded that the association of sodium and chloride to these trace metals particles was due to internal mixing of aged marine particles (311). However, they also determined a mean particle diameter larger than the size profile obtained for type Zn1. Compared to the PbZn particle type observed in Mexico City, type Zn1 (which also has Pb) appears less aged and more freshly-emitted, based on its higher intensity of phosphate and zinc chloride peaks and the lower intensity of aging markers such as nitrate (304). Type Zn3 is similar to type Zn1, though it lacks those dominant sodium and potassium peaks. In contrast, type Zn2 has ammonium [$^{+18}$NH4], zinc, zinc chloride, and nitrate, and has much larger diameters than the other two classes. The time series for all zinc types are composed mainly of sharp spikes (lasting 1 to 3 hours long) at seemingly random time periods, though the highest summer peaks generally occurred in the early afternoon. On a 24 hour basis which is typical for mass measurements, the zinc particles would appear extremely insignificant; whereas the high temporal resolution used here shows that there are short periods during which one is exposed to elevated concentrations of zinc particles. The chloride in these particles most likely originated from the same zinc sources. The presence of chlorine in waste combustion incinerators is known to influence the speciation of the metals, and chlorine compounds such as hydrochloric acid and zinc ammonium chloride, are used in hot-dip

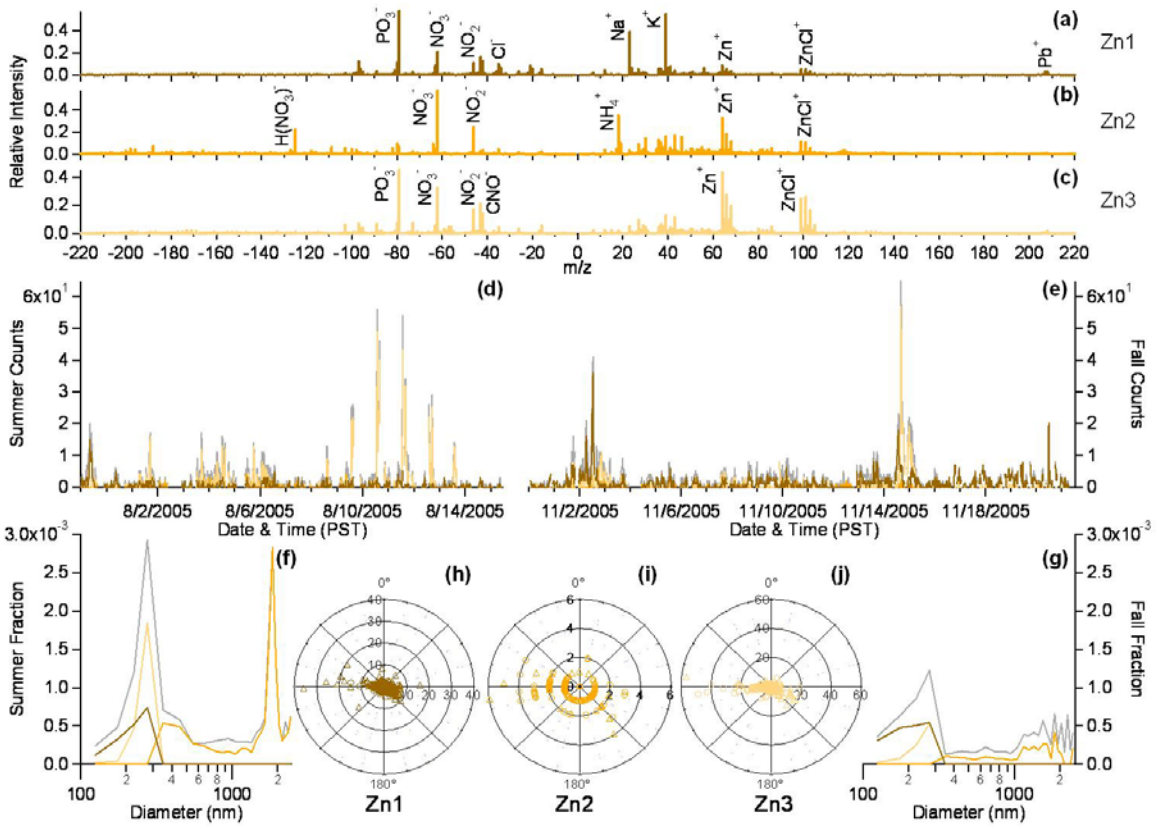

Figure 69: Trends of the three main zinc particle types: representative mass spectra (a-c); half-hourly temporal variations in summer (d) and fall (e); size-resolved total particle fractions in summer (f) and fall (g); and half-hourly wind direction profiles based on particle counts (h-j).

batch galvanizing methods (312,313). All three types generally have western wind direction preference. Interestingly, two facilities that galvanize steel materials and are among the top three facilities with reported 2005 zinc and zinc compounds emissions are located northwest of the sampling site (see **Figure 67**). These industries are the most likely source of this particle type. The fact that there is no strong seasonal dependence supports the link between these zinc particles and the galvanizing industries, because such facilities operate year round.

Barium and barium compounds are used in drilling, automotive brake pads and lubricant oils, bricks, tiles, and pesticides (314). The dominant barium class Ba1 is an organic barium particle type, containing OC, barium [$^{+138}$Ba], barium oxide [$^{+154}$BaO], barium hydroxide [$^{+155}$BaOH], chloride, nitrates, and intense peaks at m/z +59 and -101 (**Figure 70**). This unique type was also noted in Spencer et al. (48). The other barium classes contain other inorganic species, like sodium, aluminum, potassium, iron, and nitrates, and are brake dust, which is a mechanically abraded source based on their larger size distributions (315,316). The time series plots show clear seasonal differences, particularly for the organic Ba1 type; there were several consecutive summer days in which very low concentrations were detected, whereas significant concentrations were detected every day during the fall, including during the Santa Ana periods. Additionally, the high number concentrations generally were observed during the late night to early morning hours, when the wind speeds were at the lowest. Low wind speeds and the small

size of this particle type could imply a local source. The exact origin of the Ba1 type remains inconclusive.

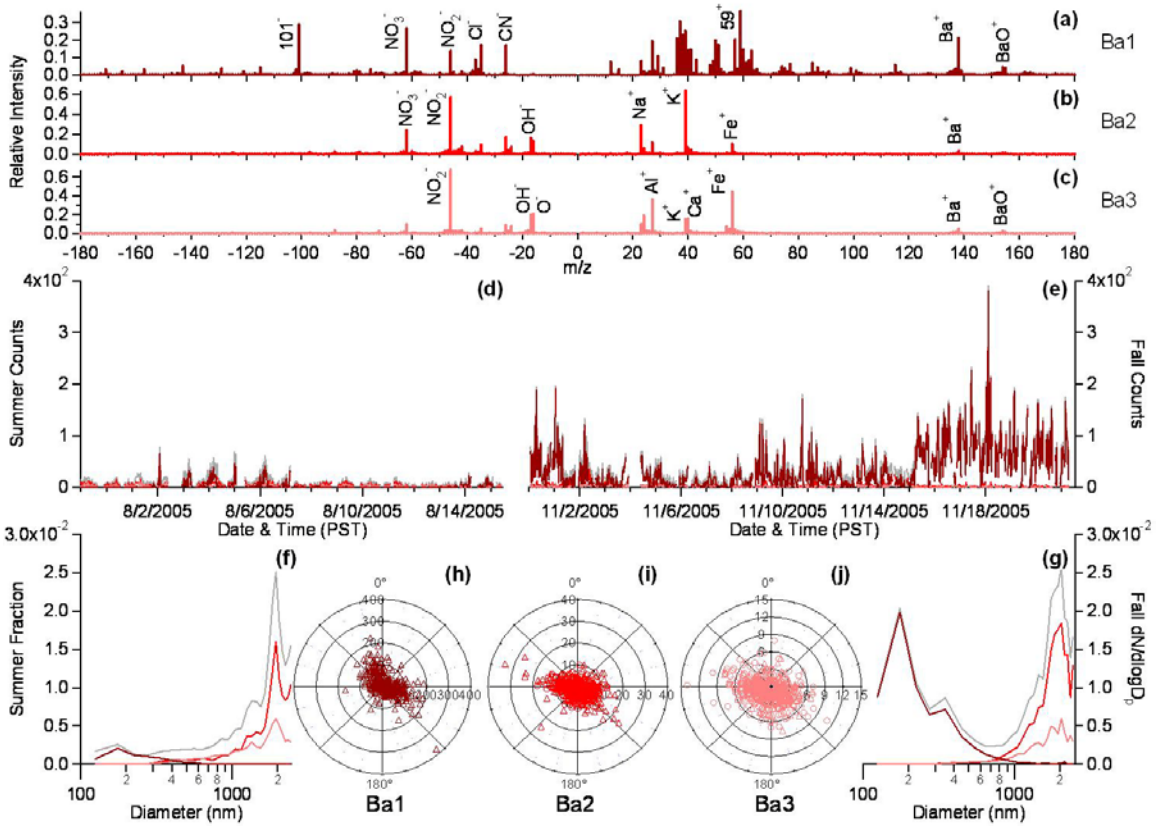

Figure 70: Trends of the three main barium particle types: representative mass spectra (a-c); half-hourly temporal variations in summer (d) and fall (e); size-resolved total particle fractions in summer (f) and fall (g); and half-hourly wind direction profiles based on particle counts (h-j).

Lead is one of the oldest known environmental toxins (records date back to 4000 years ago), and because it was used in a broad variety of products, humans are still exposed to lead on a daily basis (317). The Pb1 mass spectrum indicates an ECOC lead particle type, containing both elemental and organic carbon markers, lead, nitrates, and sulfates (**Figure 71**). The ECOC signature suggest that the Pb1 type is a combustion particle type. Types Pb2 and Pb3 are inorganic lead types, containing additional species such as sodium, potassium, iron, and nitrates. Although leaded gasoline has been phased out, the deposition of over 20,000 metric tons of lead in LA and its suburbs during the decades of its use has made the resuspension of soil a potential source of atmospheric lead in the presence and the future (318). Resuspended soil particles resemble mainly inorganic types like Pb2 and Pb3 and will generally be larger than 1 µm. Both Pb1 and Pb2 types had higher particle counts during the fall compared to the summer. These two classes both display southeast directionality, and local winds from this direction were more frequent during the fall season. **Figure 67** illustrates that over 100 facilities reported lead emissions for 2005, indicating a multitude of potential point sources for lead and the difficulty in discerning a single source. However, as both the local wind and HYSPLIT results agree that the high lead concentrations came from the east of Riverside (where there are few facilities that report lead emissions), it is clear that there is a larger source

or sources of lead than the reported anthropogenic emissions. One of the largest sources of airborne Pb in the United States is aviation gasoline [*Murphy et al.*, 2007], which is not accounted for in the point source based EPA TRI. Aircraft emissions are the likely source for the

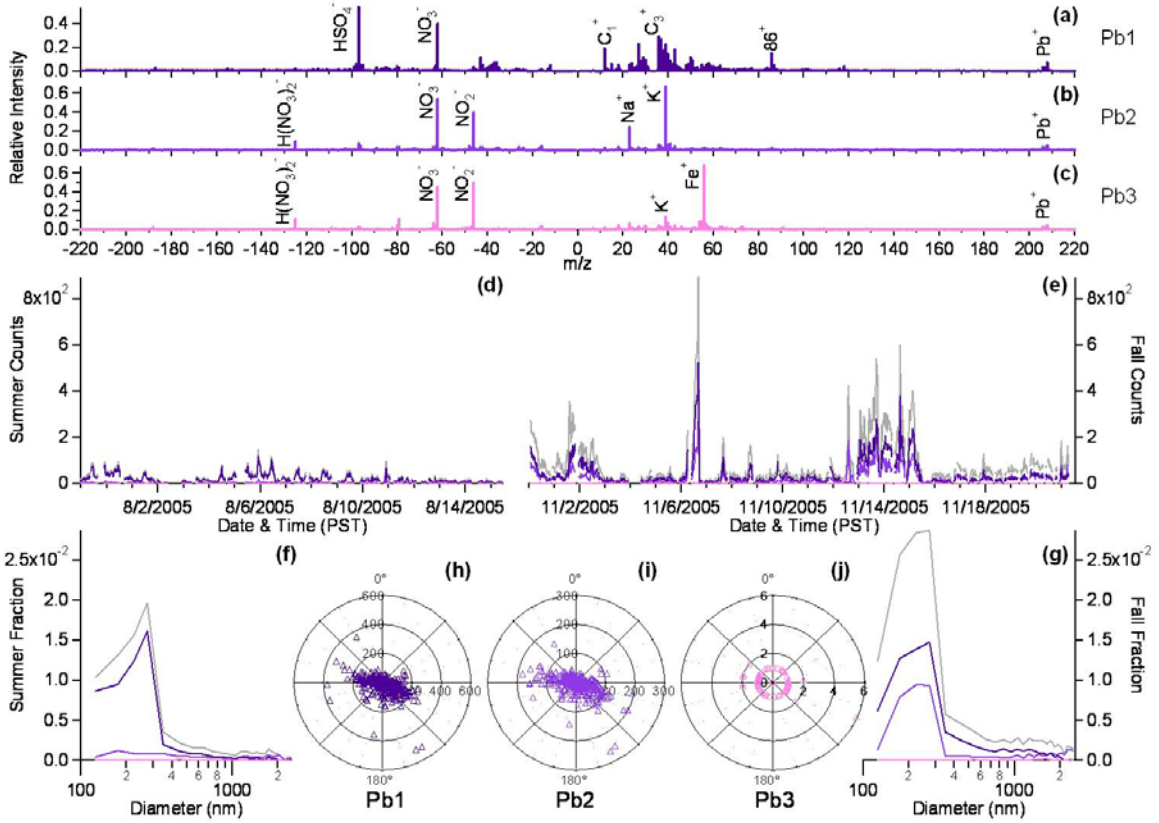

Figure 71: Trends of the three main lead particle types: representative mass spectra (a-c); half-hourly temporal variations in summer (d) and fall (e); size-resolved total particle fractions in summer (f) and fall (g); and half-hourly wind direction profiles based on particle counts (h-j).

combustion-related Pb1 type, especially considering the proximity of the local airports harboring small aircraft.

Although the analysis approach in this work focuses on the separate trace metals, it is clear that the individual particles often contain more than one trace metal. The unique combination of species provides further insights into the identification of potential sources. **Table 11** presents the percentages of metal-containing particles associated with other trace metals. For example, the V row provides the percentages of summer (S) and fall (F) vanadium-containing $PM_{2.5}$ that also have Fe, Ni, Cu, Zn, etc. All percentages greater than 5% are in bold for increased visibility. It is important to understand which metals are in the same individual particles, because the combined toxicity of metals can be greater than the toxicity of a single metal (301). Lead, as expected based on its history of broad uses, was detected in significant percentages (~20%) of several other trace metal particle types. These associations have been noted before in both Switzerland and the United States [*Murhpy et al.*, 2007]. The high correlations among vanadium, iron, and nickel also were expected based on the mass spectra described earlier. In fact, nickel was

rarely detected in a particle that did not also have vanadium, although not every vanadium particle contained nickel, particularly during the summer. Therefore, vanadium must have multiple sources, including one that also emits nickel. Interestingly, barium has very little correlation with other trace metals studied here. Because the highest percentage of another metal also associated with barium particles was only 1.7% (Fe in summer), this finding further exhibits how dominant the unique organic barium particle type was in comparison to the brake dust barium types, which both indicate the presence of iron in their spectra. Additionally, the table demonstrates some strong seasonal differences, such as the percentage of iron on copper-containing particles (1.5% versus 56.7%) and zinc-containing particles (4.6% versus 38.3%) during the summer and fall, respectively. The differences are likely a result of different sources due to the seasonal wind direction and atmospheric conditions described earlier.

	V		Fe		Ni		Cu		Zn		Sr		Mo		Sn		Sb		Ba		W		Pb	
	S	F	S	F	S	F	S	F	S	F	S	F	S	F	S	F	S	F	S	F	S	F	S	F
V			**32.0**	**70.9**	**20.4**	**72.2**	0.0	0.0	0.2	0.0	0.0	0.0	0.1	0.2	0.0	0.0	0.0	0.0	0.0	0.0	0.0	0.1	0.2	0.6
Fe	**62.8**	**75.0**			**27.5**	**66.6**	0.0	0.8	0.1	1.4	0.0	0.0	0.0	0.0	0.0	0.0	0.0	0.0	0.1	0.4	0.0	0.1	0.3	2.2
Ni	**100.0**	**99.1**	**70.1**	**86.4**			0.0	0.0	0.0	0.0	0.0	0.0	0.0	0.0	0.0	0.0	0.0	0.0	0.0	0.0	0.0	0.0	0.2	0.6
Cu	0.9	0.1	1.5	**56.7**	0.0	0.0			**6.2**	0.0	0.0	0.0	0.0	0.0	0.0	0.0	0.2	0.4	0.0	0.2	0.0	0.0	**7.4**	**16.1**
Zn	**19.1**	0.1	4.6	**38.3**	0.1	0.0	0.7	0.0			0.0	0.0	0.0	0.0	0.0	1.2	0.1	2.0	0.1	4.1	0.9	0.0	**17.6**	**23.5**
Sr	0.0	0.0	1.0	0.0	0.0	0.0	0.0	0.0	0.0	0.0			0.0	0.0	0.0	0.0	0.0	0.0	3.5	1.4	0.0	0.0	0.0	**23.1**
Mo	**33.0**	**18.0**	0.9	3.6	0.0	0.1	0.0	0.0	0.0	0.0	0.0	0.0			0.4	0.0	0.0	0.0	0.0	0.0	**5.1**	**14.3**	1.2	3.8
Sn	**11.7**	0.5	0.4	3.4	0.0	0.0	0.0	0.0	0.0	**6.6**	0.0	0.0	0.0	0.0			0.0	1.6	0.4	2.1	0.0	0.0	1.0	**14.3**
Sb	0.0	0.5	0.0	1.5	0.0	0.0	0.6	1.1	1.2	**13.2**	0.0	0.0	0.0	0.0	0.0	1.9			1.2	**6.5**	0.0	0.0	**7.1**	**21.9**
Ba	0.4	0.1	1.7	0.9	0.2	0.0	0.0	0.0	0.0	0.3	0.1	0.0	0.0	0.0	0.0	0.0	0.1				0.0	0.0	0.1	0.7
W	**7.8**	4.0	3.5	**5.5**	0.0	1.6	0.0	0.0	1.9	0.0	0.0	0.0	2.2	10.0	0.0	0.0	0.0	0.0	0.0	0.0			**42.7**	**22.7**
Pb	2.6	0.4	0.8	1.6	0.2	0.3	0.0	0.2	1.0	0.6	0.0	0.0	0.0	0.0	0.0	0.1	0.0	0.1	0.0	0.2	1.1	0.2		

S - Summer; F - Fall

Table 11: Metal association percentages (%)

In summary, the locations of potential sources and the wind direction dictate which metal-containing particles dominate during which season. In general, anthropogenic sources, mainly in the industrial and transportation sectors, in the LA Basin produced the different metal-containing particles. These observations made herein show the importance of conducting long term studies through multiple seasons to gain further understanding on how seasonal fluctuations and urban air dynamics influence

ambient particles, especially for particle types that show strong seasonal variations, such as trace metal-containing particles.

iv. Acknowledgements

The authors express their gratitude to the entire Prather group for their help in the preparation and overall support of these studies. We thank Megan McKay and the Goldstein research group at the University of California, Berkeley for the meteorology data. We also acknowledge Professor Paul Ziemann (University of California, Riverside) for hosting the SOAR field campaigns, as well as Professor Jose Jimenez (Colorado University, Boulder) and Dr. Ken Docherty (Colorado University, Boulder) for setting up the logistics. We express gratitude to the NOAA Air Resources Laboratory (ARL) for the provision of the HYSPLIT transport and dispersion model. Funding for this project was supplied by the California Air Resources Board (Contract 04-336).